The Advent of Molecular Photovoltaics and Hybrid Perovskite Solar Cells

Michael Grätzel*, Jovana V. Milić

École Polytechnique Fédérale de Lausanne, Switzerland
E-mail: michael.graetzel@epfl.ch, jovana.milic@epfl.ch

Data Availability Statement: All relevant data are within the paper and its Supporting Information files.

Competing Interests: The Author(s) declare(s) no conflict of interest.

Abstract. Over the past decade, we witnessed a remarkable development of a new generation of photovoltaic technologies, in particular dye-sensitized and perovskite solar cells. These systems have demonstrated potential to provide solutions for a more sustainable future in energy conversion. Both of these technologies, however, still encounter a number of challenges that stimulate further research. While dye-sensitized solar cells would benefit from an effective transfer from solution-based to a solid-state technology, hybrid perovskite solar cells suffer from long-term operational instability that need to be addressed. In this perspective article, we provide an overview of the recent advancements along with the perspectives for future developments.

Keywords. Molecular photovoltaics, dye-sensitized solar cells, perovskite solar cells, molecular modulation, layered hybrid perovskites.

1. INTRODUCTION

The increasing energy demands of our modern society and their impact on the environment call for novel solutions towards renewable energy conversion. One of the most auspicious technologies to meet these demands and prevent the devastating pollution caused by the combustion of fossil fuels are based on solar energy conversion.[1,2] Nature has long served as an inspiration in the ongoing quest for highly efficient light-harvesting technologies, stimulating research efforts towards sustainable energy. In natural photosynthesis, the control of molecular functions is often achieved through the role of supramolecular chemistry,[3,4] which involves fine-tuning of noncovalent interactions.[5-7] Such an approach inspired the development of a number of artificial molecular systems that convert external energy inputs into chemical energy.[5-7] In addition, natural photosynthesis has inspired the development of technologies for light-to-electrical energy conversion, in particular dye-sensitized solar cells (DSSCs).[8-12] In natural photosynthesis, the absorption of light triggers a sequential photoinduced electron transfer that contributes to the chemiosmotic gradient required to convert the electromagnetic stimuli into chemical energy that fuels the bioprocesses (Figure 1a).[3,4] Instead, in DSSCs an electrical potential gradient is generated via the photoinduced interfacial electron transfer from a molecular dye to a mesoscopic oxide, from where
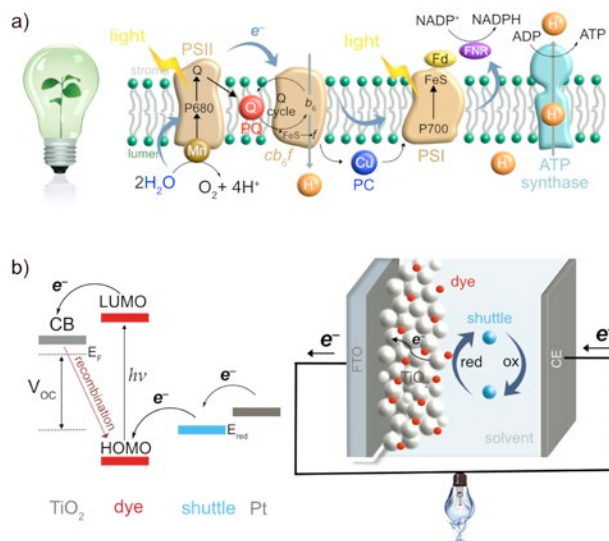
Figure 1. Schematic representation of the sequential electron transfer in (a) natural photosynthesis and (b) conventional dye-sensitized solar cells (pioneered by Grätzel at al.[8]) inspired by natural photosynthesis. PS = photosystem; ADP = adenosine diphosphate; ATP = adenosine triphosphate; NADP = nicotinamide adenine dinucleotide phosphate; NADPH = reduced NADP; Q = quinone; PQ = plastoquinone; PC = plastocyanin; P680 and P700 = chlorophyll pigments (P) of PSII and PSI, respectively, that best absorb light at either 680 nm or 700 nm, as indicated; Fd = ferredoxin; FNR = ferredoxin NADP reductase; CB = conduction band; LUMO = lowest occupied molecular orbital; HOMO = highest occupied molecular orbital; red = reduced; ox = oxidized.

it is extracted via a transparent contact to the external electric circuit. The complete cycle of converting light to electricity involves four key steps (Figure 1b): (1) photo-excitation of the light absorber (dye); (2) electron injection from the dye into the electron transport layer, commonly a mesoscopic TiO_2 or thin film transporting the charge carriers via the front contact into the external circuit; (3) dye regeneration by the redox shuttle that acts as an electron donor; and finally (4) shuttle regeneration at the counter electrode in the final step that closes the electric circuit.[10-12]

An effective solar-to-electric energy conversion requires alignment of the energy levels and favorable interaction of the participating species.[10-12] In a conventional DSSC, the redox mediator that "shuttles" electrons from the counter electrode to the photo-anode is dissolved in a liquid electrolyte. While this ascertains intimate contact with the sensitizer in the mesoporous film, it also poses limitations for industrial applications, thereby stimulating the development of solvent-free systems and solid-state technologies.[13-15] Therefore, the development of DSSCs using solvent-free ionic liquid electrolytes or solid-state hole conductors is of great interest.[13-15]

The advent of mesoscopic solar cells presented a new paradigm in photovoltaic technology as the electron- and hole-conducting materials form a three-dimensional junction, in contrast to the conventional planar p-n junctions. The prototype of this new photovoltaic family is the dye-sensitized solar cell (DSSC), also named the "Grätzel cell", which employs dye molecules, pigments or semiconductor quantum dots to sensitize a nanocrystalline wide bandgap semiconductor films. The landmark paper published in 1991 had a substantial impact being cited approximately 21'000 times until now.[8] According to an analysis by *Nature* in 2014, this publication ranks by number of citations amongst the top 100 papers of all time published across all domains of science. This revolutionary approach has allowed very high efficiencies to be reached in a photovoltaic conversion process that separated, for the first time, light harvesting and charge carrier transport, mimicking successfully the primary process in natural photosynthesis.

Ten years ago, the DSSC research became the cradle for the birth of a new closely related technology employing highly effective light absorbers known as hybrid organic-inorganic perovskites, which is referred to as perovskite solar cells (PSCs; Figure 2).[16-18] PSCs have emerged as the most promising thin-film, solution-processable, low-cost photovoltaic technology with extraordinary solar-to-electric power conversion efficiencies (PCEs) that have recently reached 25.2%, already surpassing the performance of the current market leader, polycrystalline silicon (Figure 2).[16,19-23] Unlike silicon, which is a material based on a covalent structural framework (Figure 2a),[24] hybrid perovskites are ionic crystals based on organic and inorganic components featuring mixed electronic-ionic conduction (Figure 2b).[19-26] These materials can be described by the AMX_3 formula, which is composed of a monovalent cation A (commonly methylammonium (MA) $CH_3NH_3^+$, formamidinium (FA) $CH(NH_2)_2^+$, guanidinium (GUA) $C(NH_2)_3^+$, and Cs^+), a divalent metal M (Pb_2^+, Sn_2^+), and a halide anion X (Cl^-, Br^-, I^-).[19-26] PSCs currently showing the highest performances are Pb-based comprising a mixture of different cations and halides.[22-26]

Despite their remarkable performance, however, the instability of PSCs against environmental factors, as well as under operational conditions, remains an issue that has to be addressed before practical applications become feasible (Figure 3).[27-30] This particularly refers to the sensitivity against oxygen and water, as well as heat and light stress (Figure 3a,c). Furthermore, significant effort is necessary to unravel the structure-property relationships and provide guidance for advanced material design for perovskites to reach a leading position in today's photovoltaics.[18,22]
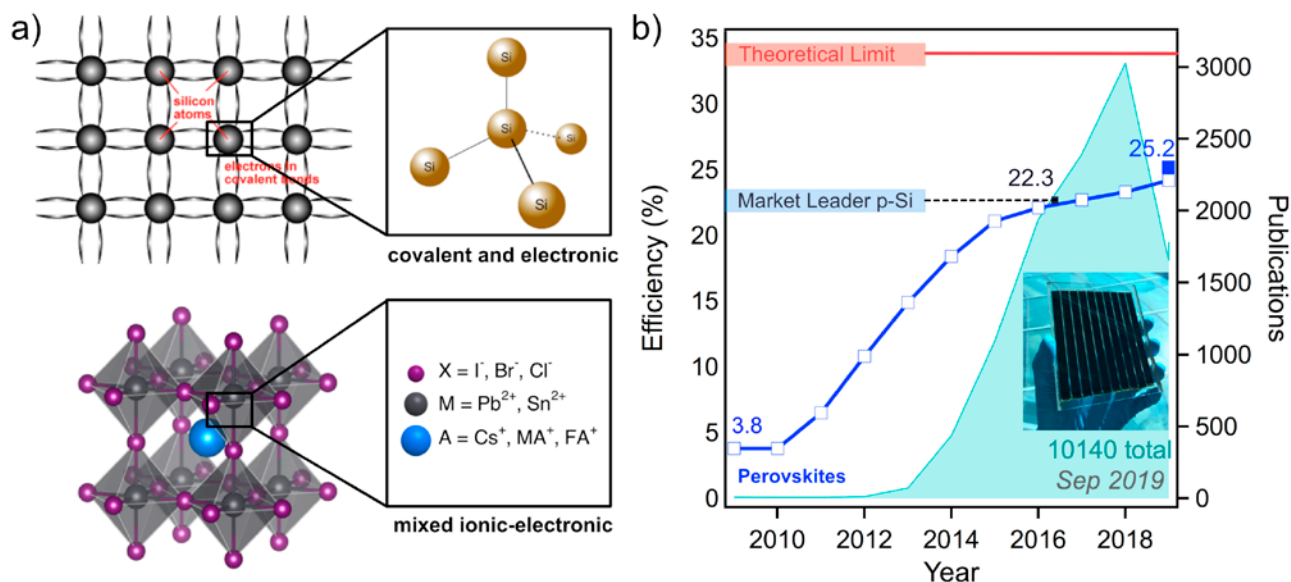
Figure 2. Structural representation of solar cell materials and the evolution of their performance. (a) Schematic representation of the structure of silicon (upper; figure adapted from ref.[24]) and hybrid perovskites (lower) with the chemical formula AMX$_3$. (b) Evolution of the photovoltaic performance of PSCs since 2009 (blue) in comparison to polycrystalline silicon (22.3% efficiency) and the theoretical limit (red), with the corresponding number of publications on hybrid perovskite solar cells (based on the Scopus analysis for the term "perovskite solar cell" on September 23, 2019). In 2019 the efficiency of PSCs has reached 25.2%.[16] A representative photo of a perovskite solar cell is shown in the inset (photo credit to the researchers at NTU Singapore).
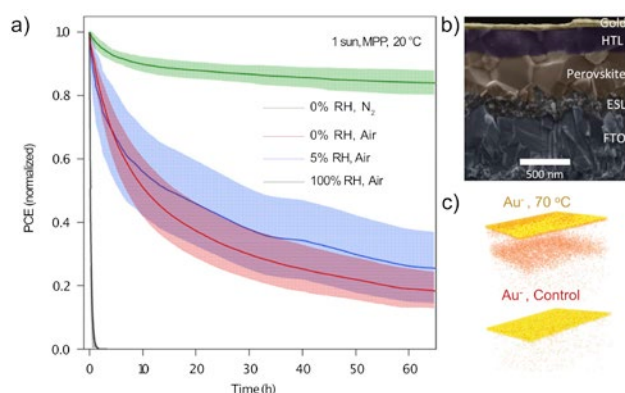

Figure 3. Aging of typical triple cation double halide perovskite solar cells. (a) Evolution of solar-to-electric power conversion efficiency under operational stability conditions upon continuous irradiation by maximum power point (MPP) tracking. Adapted with permission from ref.[30] (b) Cross-sectional scanning electron microscopy (SEM) image of a typical PSC highlighting its architecture and (c) time of flight secondary ion mass spectroscopy elemental depth profiling image showing the concentration of Au species across the device, indicative of ion migration under operational conditions at elevated temperatures. Adapted with permission from ref.[30] Copyright 2016 American Chemical Society.

In contrast to three-dimensional (3D) perovskites, their layered two-dimensional (2D) analogues have demonstrated promising environmental stability.[31-35] These materials are often described by the general $S_2A_{n-1}M_nX_{3n+1}$ formula. Here, species S (typically $C_mH_{2m+1}NH_3^+$) and A (typically MA, FA, or their mixtures) are organic cations, M is a divalent metal cation (Pb^{2+}, Sn^{2+}), X is a halide ion (Br$^-$, I$^-$), and the value n represents the number of layers of $[MX_6]^{4-}$ octahedra in the hybrid perovskite phase. The structure consists of layers of perovskite slabs separated by the organic ammonium cation spacers (Figure 4).[35] The spacer cation defines the properties of the layered 2D perovskites and consequently, the corresponding optoelectronic device performance.[36] The most commonly used spacers feature hydrophobic alkyl chains, such as n-buthylammonium (BA) or phenylethylammonium (PEA), which are essential to increasing the resilience of the material against the environmental factors. This contribution to the stability, however, comes at the expense of the solar-to-electric power conversion efficiency, which requires further advancement of these materials and the corresponding devices.[31]

2. RECENT ADVANCEMENTS OF DYE-SENSITIZED SOLAR CELLS

The inception of dye sensitized solar cells (DSSC) about 30 years ago by the Grätzel group provoked a revolution in photovoltaics.[8] He is credited with moving the
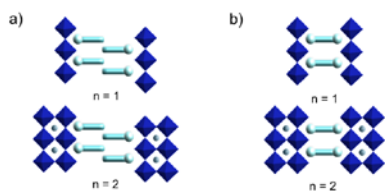
Figure 4. Structural representation of layered two-dimensional perovskites. Schematic of (a) $S_2A_{n-1}Pb_nI_{3n+1}$ (Ruddlesden-Popper, RP), (b) $SA_{n-1}Pb_nI_{3n+1}$ (Dion Jacobson, DJ) formulations with different number of inorganic layers (n). Blue octahedra illustrate the $\{PbI_6{}^{4-}\}$ units, light blue spheres the A cations, whereas the cyan and green rods correspond to the organic spacers (S, S').

solar cell field beyond the principle of light absorption via diodes to the molecular level, exploiting the sensitization of wide bandgap semiconductor oxides by the dye molecules, pigments or semiconductor nanocrystals for light energy harvesting. The key to this success was the introduction of a new paradigm in photovoltaics. Instead of using the conventional planar p-n junction cell architecture, a 3D scaffold of semiconducting oxide nanoparticles was introduced in order to collect the electrons injected into the conduction band by the monolayer of adsorbed sensitizer molecules. The stacking of the nanoparticles produced a mesoscopic film with very high internal surface area, which enabled efficient light harvesting by the sensitizer. By contrast, on a flat surface, a self-assembled monolayer of molecular dye produces a very week photo-response, since the light absorption cross-section of a molecule is several orders of magnitude smaller than the area it occupies. Introducing a 3D mesoporous semiconducting oxide film as electron selective contact to support the sensitizer overcame this fundamental problem. As a result of its large internal surface area, the film achieves very efficient light harvesting even at monolayer surface coverage by dyes or semiconductor quantum dots. This, nevertheless, left the challenge to find a way to collect the electrons injected by the sensitizer into the nanoparticle network before they recombine with the positive charges left behind on the sensitizer. This task appeared to be particularly arduous in view of the fact that the charge carrier collection was not assisted by an electric field of the type present in a conventional planar p-n junction device.

Judicious molecular engineering of sensitizers enabled to address this challenge and to realize chromophores that would sustain the light-induced charge separation across the interface for long enough time to collect the photo-injected carriers before they were recaptured by the dye or by the oxidized form of the redox mediator. This development was supported by computational analysis, which provided precious help in the conception, design and synthesis of the best performing sensitizers.[37-41] Examples of some of the structures of the molecules that have emerged as some of the most powerful DSSC sensitizers and redox shuttles are shown in Figure 5. Due to their outstanding stability and broad visible light absorption, the bis-thiocyanato ruthenium bipyridyl complexes became the sensitizer of choice and are currently produced on the multi-kilogram scale for use in commercial products. The scaleup in production has lowered their prize by a factor of 100, from initially over 1000 US$/g to 10 US$/g, rendering DSSCs competitive with conventional systems. Today, we witness the emergence of organic and semiconductor quantum dots as sensitizers, which show superior light-harvesting properties to the ruthenium dyes. In-depth theoretical and experimental studies elucidated the fundamental features of the dynamics of interfacial electron transfer and charge carrier recombination within and at the surface of the semiconductor oxide nanocrystals. Laser photolysis in conjunction with time-resolved spectroscopy at the femtosecond time domain showed that judicious design of the sensitizer molecule allows to control the rate of the interfacial electron transfer reactions. For state-of-the-art sensitizers, the electron injection in the conduction band of TiO_2 scaffold occurs on the femtosecond to picosecond timescale, while the charge carrier recombination takes milliseconds or even seconds. This is sufficiently long to allow for near-quantitative collection of the photo-generated charge carriers as electric current. These molecular systems can generate photocurrents that were about 10'000- times larger than those obtained with planar architectures, converting over 90% of the incoming photons into the electric current within the absorption wavelength range of the sensitizer. The very efficient conversion of sunlight with molecular chromophores renders the DSSCs the first photovoltaic technology to mimic the light reaction in natural photosynthesis. This presents one of the most exciting developments in the generation of renewable energy from solar power.

A further advancement of DSSCs was made through the molecular engineering of a new donor-acceptor porphyrin sensitizer, coded YD2, achieving an efficiency record of 12.4 % when employed with a cobalt complex as redox shuttle (Figure 5).[42] Due to its beautiful green colour and its high efficiency, this sensitizer is presently upscaled for powering DSSC-based glazing (Figure 6). An example is the green sound protection barrier installed on the highway between Bern and Zurich that produces over 1000 kWh/year of electricity (Figure 6). Further computation-assisted molecular engineering of this type of donor-acceptor porphyrins allowed realizing panchromatic light harvesting across the whole visible spectrum, increasing the PCE to 13%.[43]
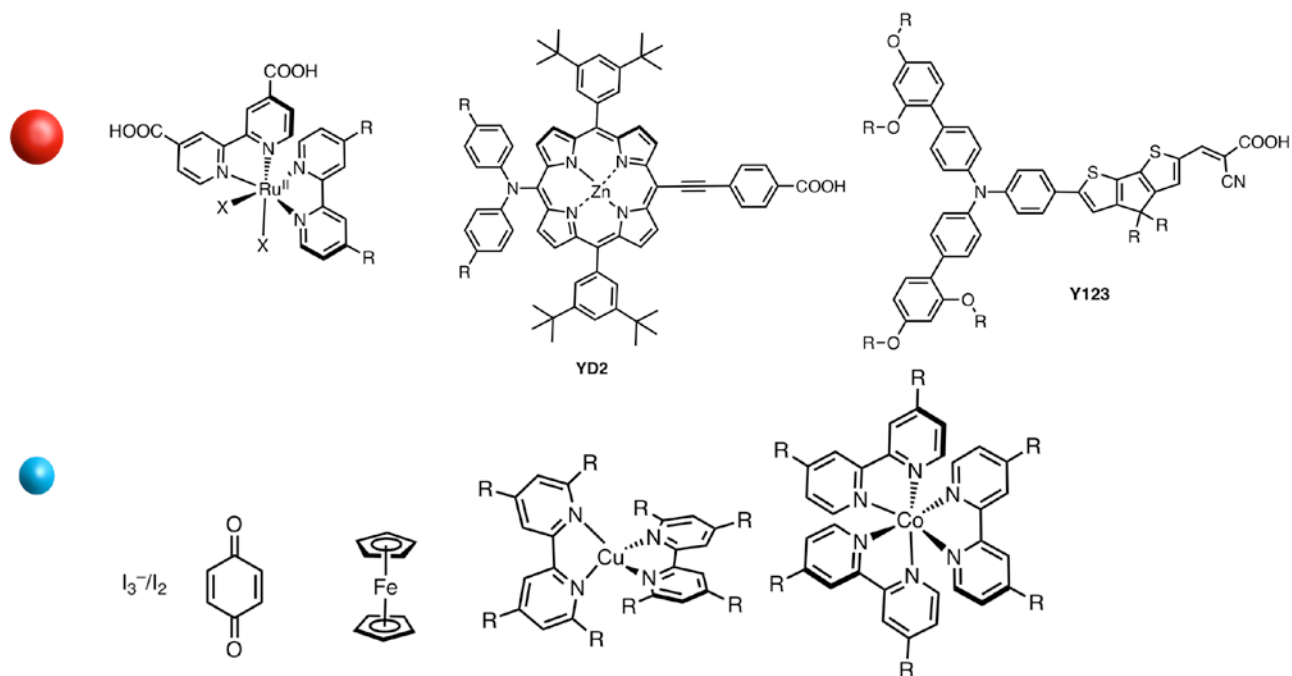
Figure 5. Structures of dye molecules (red) and redox shuttles (blue) commonly employed in DSSCs. Their roles are schematically illustrated in Figure 1b. R represents various alkyl/alkoxy substituents while X = SCN.

Ionic liquids played a crucial role as non-volatile, solvent-free redox electrolytes, enabling the practical deployment of DSSCs. New hydrophobic ionic liquids were developed displaying low viscosity, which have found widespread applications and are now produced commercially.[44] Substantial advances in performance were achieved by introducing eutectic mixtures of imidazolium iodide salts as redox active ionic liquids, where the charge transport is accelerated by a Groothus-type exchange mechanism.[45] The breakthroughs made in this area have dramatically increased the stability of DSSCs under prolonged light soaking and heat stress, fostering their practical development for outside deployment. Several companies are now manufacturing ionic liquid based on DSSCs on a commercial scale.

Solid-state dye sensitized solar cells are the main focus of current research efforts. Taking the inspiration from the work of C. Tang on organic light-emit-
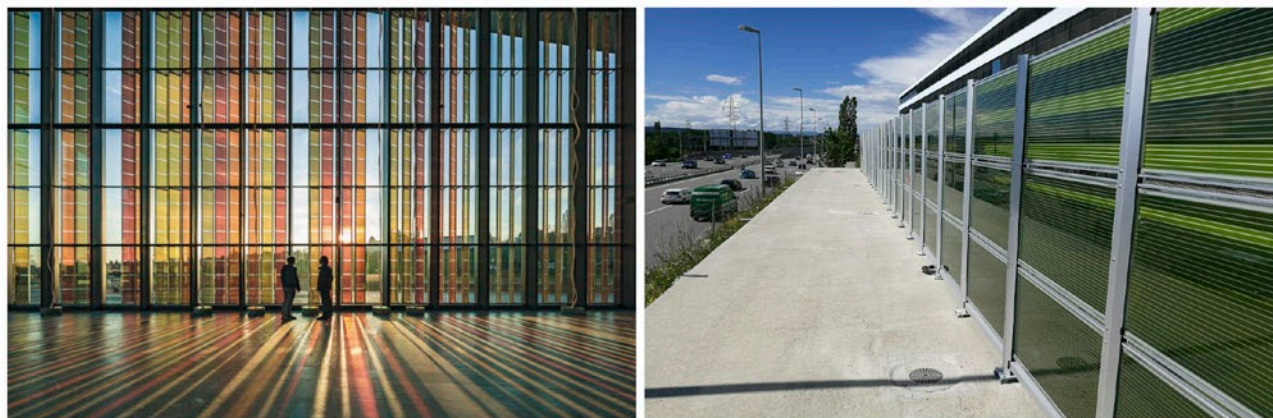
Figure 6. Examples for DSSC-based photovoltaic glazing. Left: DSSC panels produced by the company Solaronix (www.solaronix.ch) mounted at the façade of the Swiss High-Tech Convention Centre in Lausanne, Switzerland. Right: The first energy-producing noise-barrier based on the DSSC panels developed by the Swiss company H.Glass is installed on the highway between Bern and Zurich in Switzerland.
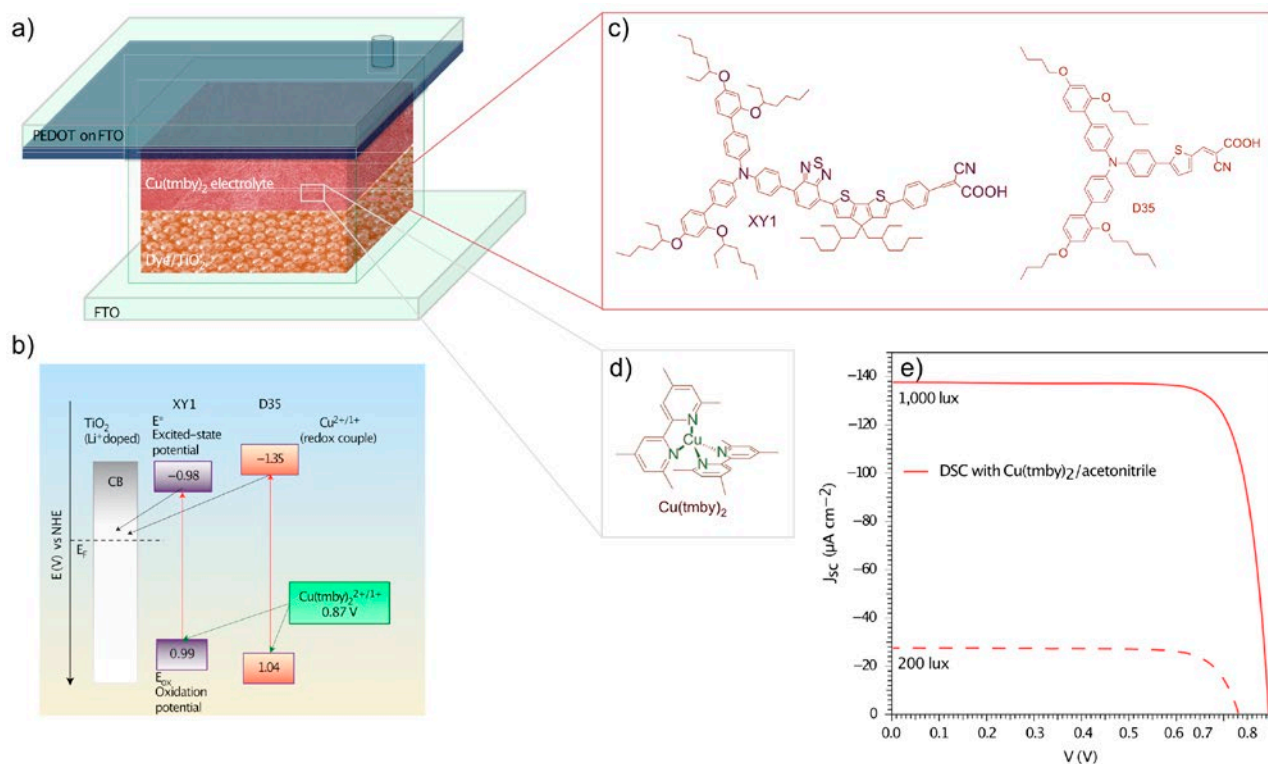
Figure 7. Example of a Cu-based dye-sensitized solar cell. (a) Schematic representation of the device architecture and (b) energy alignment of the device components, with the structure of the corresponding (c) dyes and (d) redox shuttle, as well as the (e) current-voltage characteristic at different light intensities. Adapted from ref.[47] with permission. tmby = 4,4',6,6'-tetramethyl-2,2'-bipyridine; PEDOT = poly(3,4-ethylenedioxythiophene); FTO = fluorine-doped tin oxide.

ting diodes, Grätzel et al. replaced the liquid electrolyte by solid organic hole conductors. Specifically, his group introduced the triarylamine derivative, namely 2,2',7,7'-tetrakis(N,N-di-pmethoxyphenylamine)-9,9-spirobifluorene (spiro-MeOTAD), as a hole-transporting material, which is now widely applied.[46] Starting from low efficiencies below 1%, the PCE of solid-state DSSCs reaches presently over 11% using a solid-state Cu(II)/Cu(I) redox system for hole conduction. The advantage of employing a solid-state hole conductor is that it is non-volatile, showing faster charge carrier transport, while chemically less aggressive than a redox electrolyte. Hence, further research on solid-state DSSCs is presently being actively pursued. This development served as a springboard for the recent stunning rise of perovskite solar cells using the mesoscopic architecture of solid-state DSSC and hole conductors based on the spiro-MeOTAD family.

DSSCs based on Cu complexes as redox shuttles have taken the lead in electric power generation from ambient lighting.[47] Ambient light-harvesting systems are of great practical interest, as they can serve as elec-

tric power sources for portable electronics and can render the operation of a great variety of devices for wireless sensor networks (WSN) or IoT (Internet of Things) autonomous. A new DSSC embodiment has recently been shown to achieve high power conversion efficiencies (PCE) under ambient light conditions (Figure 7a,b). The photosystem combines two judiciously designed sensitizers coded D35 and XY1 (Figure 7c), with the copper complex Cu(II/I)(tmby) as redox shuttle (tmby = 4,4',6,6'- tetramethyl-2,2'-bipyridine; Figure 7d), which quantitatively regenerates both dyes at a very low driving force, resulting in open circuit photovoltages (V_{OC}) up to 1.1 V (Figure 7e). The electric power production at 1000 lux exceeded the PCE of GaAs under similar conditions, highlighting the potential of this technology.

3. RECENT ADVANCEMENTS OF HYBRID PEROVSKITE SOLAR CELLS

Since the first demonstration of the hybrid perovskite solar cell in 2009 by Miyasaka et al., the performance of this technology has rapidly evolved from

PCE of 3.8% to over 25% in just a decade, which has been unprecedented in photovoltaics (Figure 2b).[16,18,23,48] While this progress has been remarkable, PSCs continue to face obstacles to their application, which are mainly related to their instability against moisture and oxygen, as well as light and heat stress under operational conditions.[48,49] In addition, the progress in hybrid perovskite research has been primarily driven by the device performance, while the underlying degradation mechanisms and structure-property relationships remain poorly understood, which prevents rational material design required for further advancement.[48,49] To overcome these challenges, a number of strategies emerged over the past years with promising future prospects. Amongst these, three strategies related to the material design are particularly important (Figure 8), namely (1) compositional engineering, (2) employing a variety of modulators to the perovskite composition to alter their properties[50,51] as well as (3) layered two-dimensional perovskites and their heterostructures.[52,53] This progress was accompanied by the development of the analytical tools based on solid-state nuclear magnetic resonance (NMR) spectroscopy to unravel the structural properties at the atomic level and guide rational material design.[54-59]

Compositional engineering played a pivotal role in advancing PSCs since the properties of hybrid organic-inorganic halide perovskite materials are strongly dependent on their composition. This progress was facilitated by several major advancements. Following the first attempts to employ hybrid perovskite materials based on methylammonium (MA) cation,[60] Eperon et. al.[61] introduced the formamidinium (FA) to reduce the band gap from 1.53 eV to 1.48 eV and consequently increase the theoretical performance limit. However, the performance of FA-based compositions were lower than that of MA-based ones, since the perovskite-type $FAPbI_3$ polymorph (α-$FAPbI_3$) is not thermodynamically stable at temperatures below 150 °C and it transforms into the yellow polymorph (δ-$FAPbI_3$) under ambient conditions.[62] Phase stability of the mixed FA/MA compositions were improved by gradually substituting MA with FA cations,[19] and the utility of FA-based systems was further stimulated by their enhanced stability at elevated temperatures.[63,64] This approach of mixing cations in hybrid perovskites was advanced further by introducing 15% $MAPbBr_3$ in $FAPbI_3$ to reach PCEs above 18%.[65] Furthermore, Cs^+ was introduced into the composition to define the commonly employed triple cation $Cs_{0.05}MA_{0.17}FA_{0.83}Pb(I_{0.83}Br_{0.17})_3$ perovskite formulation, which provided a more reproducible and stable composition for PSCs reaching PCE beyond 21%,[25] and later on beyond 22% by reducing the bromide concentration.[17] Further progress in achieving the efficiencies that exceed 23% was reached through interfacial engineering[66] and by
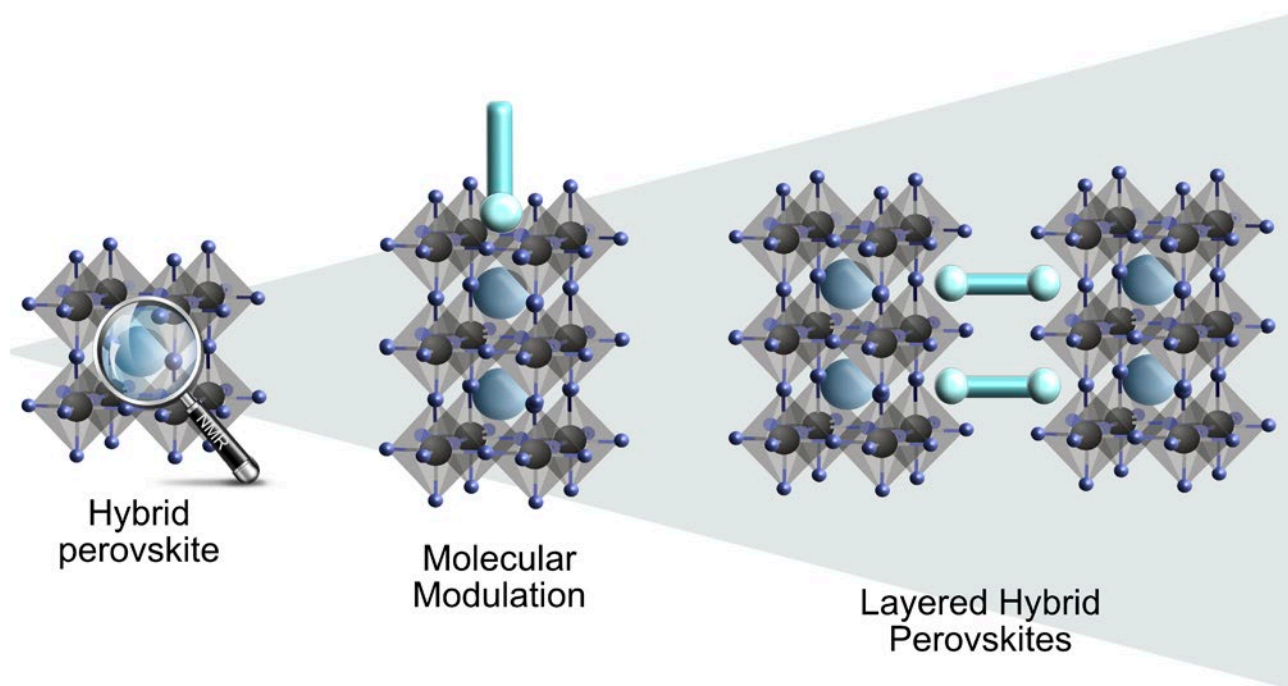
Figure 8. Gradual evolution of hybrid perovskite materials. Schematic representation of development through compositional engineering and molecular modulation to the layered hybrid perovskite materials.
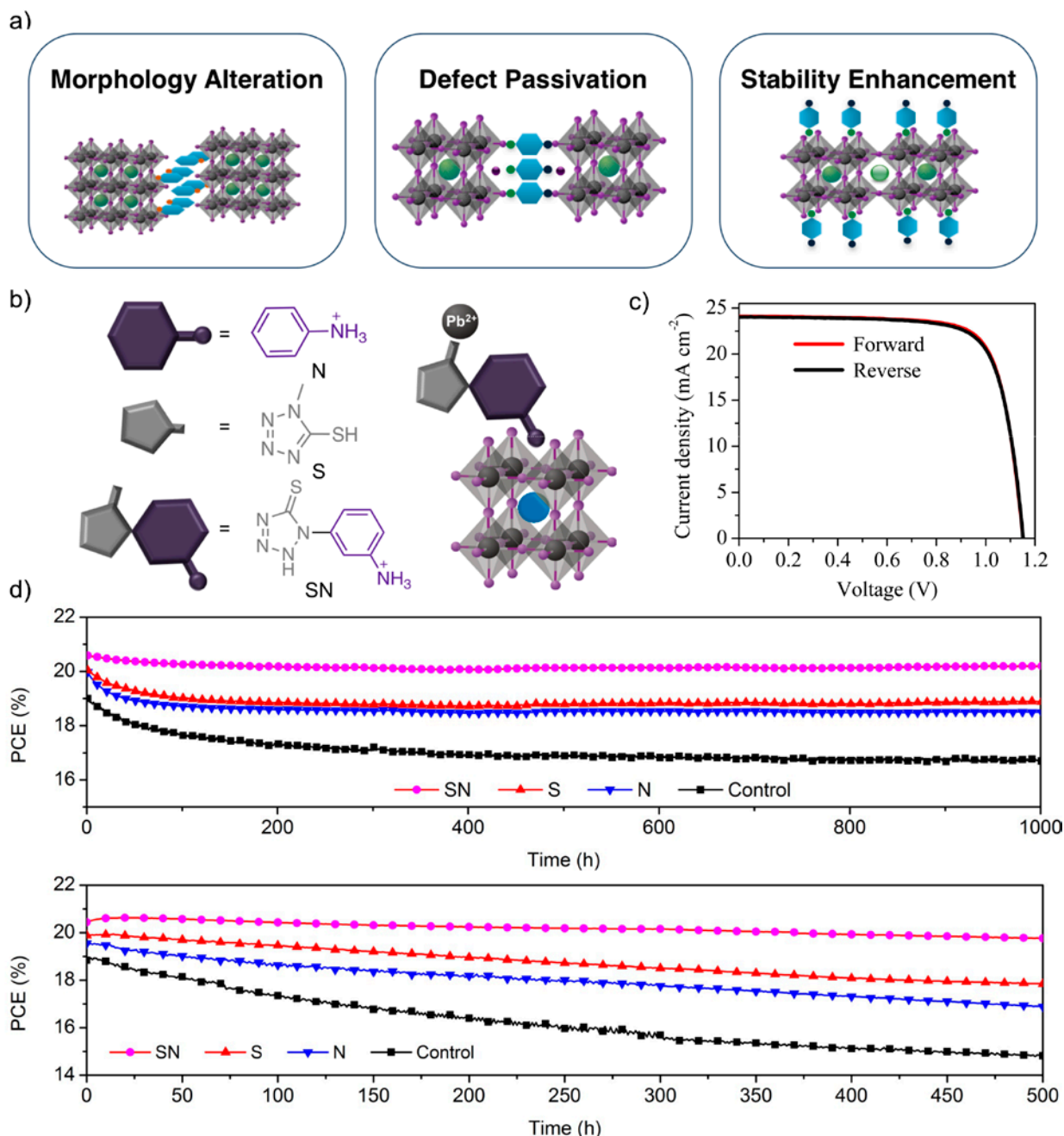
Figure 9. Molecular modulation case. (a) Overview of effects of molecular modulation on hybrid perovskite solar cells: morphology alteration, defect passivation, and stability enhancement. Adopted with permission from ref.[51] (b) Example of molecular modulators **N** (purple), **S** (grey), and **SN** (purple-grey) with a schematic representation of the interaction of **SN** with Pb^{2+} ions (grey sphere) and the hybrid perovskite (FAPbI$_3$). (c) J-V curves of the modulated champion device recorded in reverse (black; from V_{OC} to J_{SC}) and forward (red; from J_{SC} to V_{OC}) scanning directions under AM 1.5G solar radiation. (d) Evolution of power conversion efficiency of devices over time upon continuous light illumination at 65 °C and maximum power point tracking under argon (upper) and ambient air (lower) conditions. Adapted from ref.[76]

employing either molecular modulation or layered two-dimensional hybrid perovskite heterostructures.[67]

Molecular modulation refers to utilising organic molecules within the hybrid perovskite composition with the aim of addressing a specific function at the molecular level.[51] Three functional areas are particularly relevant for molecular modulation (Figure 9a), namely morphology alteration,[68-70] passivation of defects that

might act as recombination centers,[71-73] and stabilization of the perovskite structure against the environmental factors as well as by suppression of the internal ion migration.[74,75] Milic and Grätzel et al. have shown that addressing these functional areas requires strategies that are based on purposefully tuning a variety of noncovalent interactions that can be employed to alter the morphology, passivate the defects, as well as self-assemble layers for either encapsulation or suppressing the detrimental ion migration.[51] For instance, a bifunctional modulator, 3-(5-mercapto-1*H*-tetrazol-1-yl)benzenaminium iodide (**SN**), was developed comprising of the anilinium core (**N**; purple in Figure 9b) that act as a hydrogen-bond-donating group for interaction with the surface of the hybrid perovskite and a thiol-tetrazolium unit (**S**; grey in Figure 9b) to coordinate the Pb^{2+} cations that can act as recombination centres.[76] These functional groups are used as part of a hydrophobic aromatic scaffold introduced with the objective of enhancing the tolerance to environmental factors. As a result, adding the modulator to the perovskite precursor solution and treating the surface of the thin films provided a beneficial effect on the optoelectronic properties. This was evidenced in photovoltaic devices of conventional mesoscopic Au/spiro-OMeTAD/perovskite/mesoporous-TiO_2/compact-TiO_2/fluorine-doped tin oxide (FTO) architecture, which were measured under conditions of standard AM 1.5G illumination at light intensity of 100 mW cm^{-2} (Figure 9c–d). The devices demonstrated an improvement of the photovoltaic performance as compared to the pristine (control) samples, including an increase of the short circuit current density (J_{SC}), open-circuit voltage (V_{OC}), fill factor (FF), and the PCE (Figure 9 c–da). The J_{SC} improvements are ascribed to the higher electronic quality of the films and effective charge collection, whereas increased V_{OC} stems from the suppression of charge carrier recombination upon defect passivation.[51] This resulted in PCEs exceeding 20% PCE, with J_{SC} of 24 mA cm^{-2}, V_{OC} 1.15 V, and FF up to 0.75 (Figure 9c) for double cation single halide perovskite-based devices. Moreover, the exceptional performance was accompanied by a long-term stability upon continuous illumination at elevated degradation conditions between 55–60 °C in either argon atmosphere or humid ambient air (Figure 9d).[76] This enhancement in stability and performance upon modulation corroborates the suppression of morphological changes upon aging, as well as passivation of defects, in addition to an increase in hydrophobicity that was evidenced by contact angle measurements.[76]

Such effects of the modulation on the properties of hybrid perovskites are not limited to this modulator or a single perovskite composition.[51] The atomic-level interactions responsible for this function can be analysed by solid-state NMR spectroscopy, which sets the basis for advanced molecular design.

Solid state NMR spectroscopy is a powerful technique that provides atomic-level information about the microstructure of the material. It has been successfully employed to scrutinize the incorporation of the variety of organic and inorganic cations into the hybrid perovskite structure.[54-57] In particular, the comparison of ^{13}C, ^{14}N, and ^{15}N magic angle spinning (MAS) NMR spectra of neat mechanochemical α-FAPbI$_3$ and bulk mixtures with sub-stoichiometric amounts of modulators provide unique structural insights.[54-58] This involves identifying the interaction between the modulator and the hybrid perovskite, assessing whether it involves incorporation of the modulator insight the A cation site, as well as whether the interaction induces any changes in the perovskite crystallographic properties (Figure 10).

The interaction between the modulator and the perovskite can be evidenced by the appearance of new NMR resonances in the mixtures prepared mechanochemically.[51,76] For instance, a comparison between the ^{13}C NMR spectra of the **SN**-modulated α-FAPbI$_3$ perovskite (Figure 10a) and the neat modulator (Figure 10b) reveals a set of additional carbon environments, which can be associated with the **SN** interacting with the perovskite. The chemical shifts can also provide more information about the interaction and scrutinize the propensity of the modulator to incorporate into the corresponding A cation sites. In this regard, the ^{13}C and ^{15}N NMR spectra of the neat and **SN**-modulated α-FAPbI$_3$ material reveals similar ^{13}C and ^{15}N resonances (Figure 10c,d and Figure 10e,f), which suggests that **SN** does not incorporate into the perovskite lattice. However, a small (0.2 ppm) in the NMR spectra upon modulation evidences structural differences between the two materials, which points at the interaction taking place on the surface of the hybrid perovskite instead. Such interaction can result in the changes in the crystallographic properties of the hybrid perovskite, which can be uniquely probed by ^{14}N NMR spectroscopy. This is due to the dependence of the breadth of the residual ^{14}N spinning sideband (SSB) manifolds on the reorientation of FA inside the cuboctahedral cavity that is related to the symmetry of cation reorientation. Specifically, narrower ^{14}N SSB manifolds correspond to higher symmetry that is closer to cubic.[54] The ^{14}N MAS NMR spectra of neat (Figure 10g,i) and modulated α-FAPbI$_3$ (Figure 10h,j) show a SBB pattern that becomes narrower in the modulated material. This means that the modulation of α-FAPbI$_3$ phase increases its crystallographic symmetry,
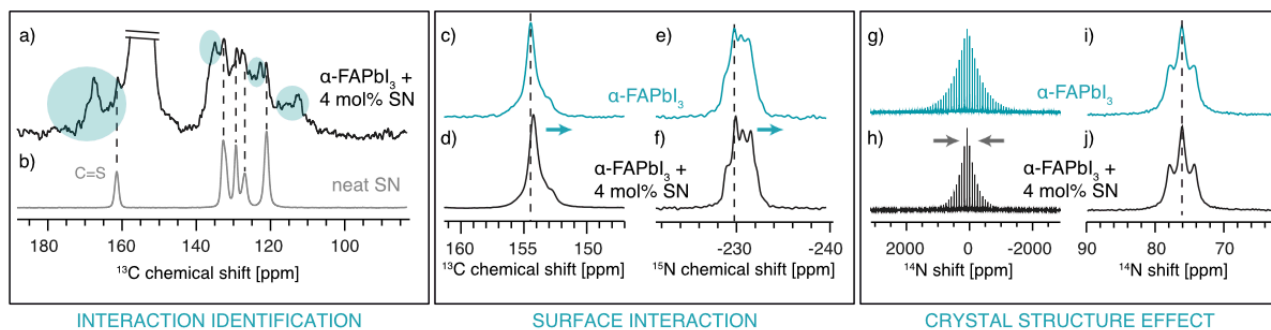
Figure 10. Probing molecular modulation at the atomic level by solid-state NMR spectroscopy. (a−b) Identifying interactions via ^{13}C cross-polarization (CP) solid-state magic angle spinning (MAS) NMR spectra at 11.7 T, 105 K, 10 kHz MAS of a) neat mechanochemical α-FAPbI$_3$ with 4 mol% **SN** and b) neat **SN**. Blue circles showcase the new environments that are associated with the interaction of the modulator. (c−f) Minor changes in the chemical shift (0.2 ppm) highlighted by the blue arrows of the ^{13}C CP and ^{15}N CP solid-state MAS NMR spectra at 11.7 T, 105 K, 10 kHz MAS of neat mechanochemical c,d) α-FAPbI$_3$ and e,f) α-FAPbI$_3$ with 4 mol% **SN** suggest that the interaction takes place on the surface of the hybrid perovskite as opposed to by A-cation incorporation. (g−j) Changes in the crystal structure of FAPbI$_3$ revealed by ^{14}N solid-state MAS NMR spectra at 11.7 T, 298 K and g,h) 3 kHz and i,j) 20 kHz MAS of bulk mechanochemical g) α-FAPbI$_3$ and h) α-FAPbI$_3$ with 4 mol% SN implied by narrowing of the SBB manifold (grey arrows). Panels i,j) shows the views of the center band. Adapted from ref.[51,76]

rendering it closer to cubic. Moreover, the peak features the same shift in both samples, which supports the conclusion that the change is not caused by incorporation of the modulator into the A cation site but rather a result of a surface interaction.[51,76]

Similarly, the interaction of the modulators with the potential defects, such as PbI$_2$, can be probed, which can serve to unravel the likelihood of defect passivation. This role of molecular modulators in directing the structure of hybrid perovskites and passivating some of the defects was found to benefit the device performance and stability even for the substoichiometric amounts of the modulator. Such molecular-level engineering assessed by solid-state NMR spectroscopy sets the stage for more elaborate material design with further enhanced stability, such as in the layered hybrid perovskites.

Layered hybrid perovskites fully incorporate the organic component within the layers of hybrid perovskite slabs. Following the pioneering work of Mitzi et al.[77] a number of layered perovskite materials were developed over the past years. While these systems can stabilize the perovskite structure, particularly against the detrimental effect of humidity, the performances of the resulting solar cells remain inferior to those of their 3D analogues. This can be attributed to the charge transport inhibition by the organic cations that act as insulating layers, since the inorganic domains mainly contribute to the electronic charge transport.[52,53] Moreover, they feature a larger exciton binding energy that results in the decrease of the performance that is often related to the short circuit current losses owing to inefficient exciton dissociation.[35] This can be circumvented by tuning the organic cation groups[35]

or by employing hot-casting fabrication techniques.[31] A unique advantage of tunability of the properties based on the molecular design of organic spacer cations permits to rely on hydrophobic chains and van der Waals interactions between the adjacent layers to contribute to the stability, without compromising the crystallinity of the material.[32] Commonly employed organic cations, such as the BA or PEA, which form Ruddlesden-Popper perovskite phases, feature long alkyl chains that jeopardize the crystallinity of the materials.[35,36] Further engineering of the noncovalent interactions within the spacer layer has the propensity to boost the performances of this category of perovskites and the supramolecular strategies are underutilized in this context.

In order to demonstrate the potential for exploiting the Van der Walls interactions of the spacer layer, for instance, A$_2$FA$_{n−1}$Pb$_n$I$_{3n+1}$ (n = 1–4) compositions based on the (adamantan-1-yl)methanammonium (A) as a spacer were developed (Figure 11). Adamantane is a well-known building block in supramolecular chemistry that features ordered self-assembled structures based on Van der Waals interactions.[78-83] In addition, the high symmetry and dynamics of functional adamantane systems is known to be used in plastic crystals and molecular machines.[84] The utility of these systems was probed in the A$_2$FA$_{n−1}$Pb$_n$I$_{3n+1}$ formulations based on thermally stable FA-based perovskite compositions by using stoichiometries with different numbers of layers (n = 1 – 4) separated by the spacer. The unique property of layered 2D perovskites is that they behave as natural quantum wells that feature a gradual decrease in the bandgap (E_g) with an increase in the number (n) of inorganic layers,
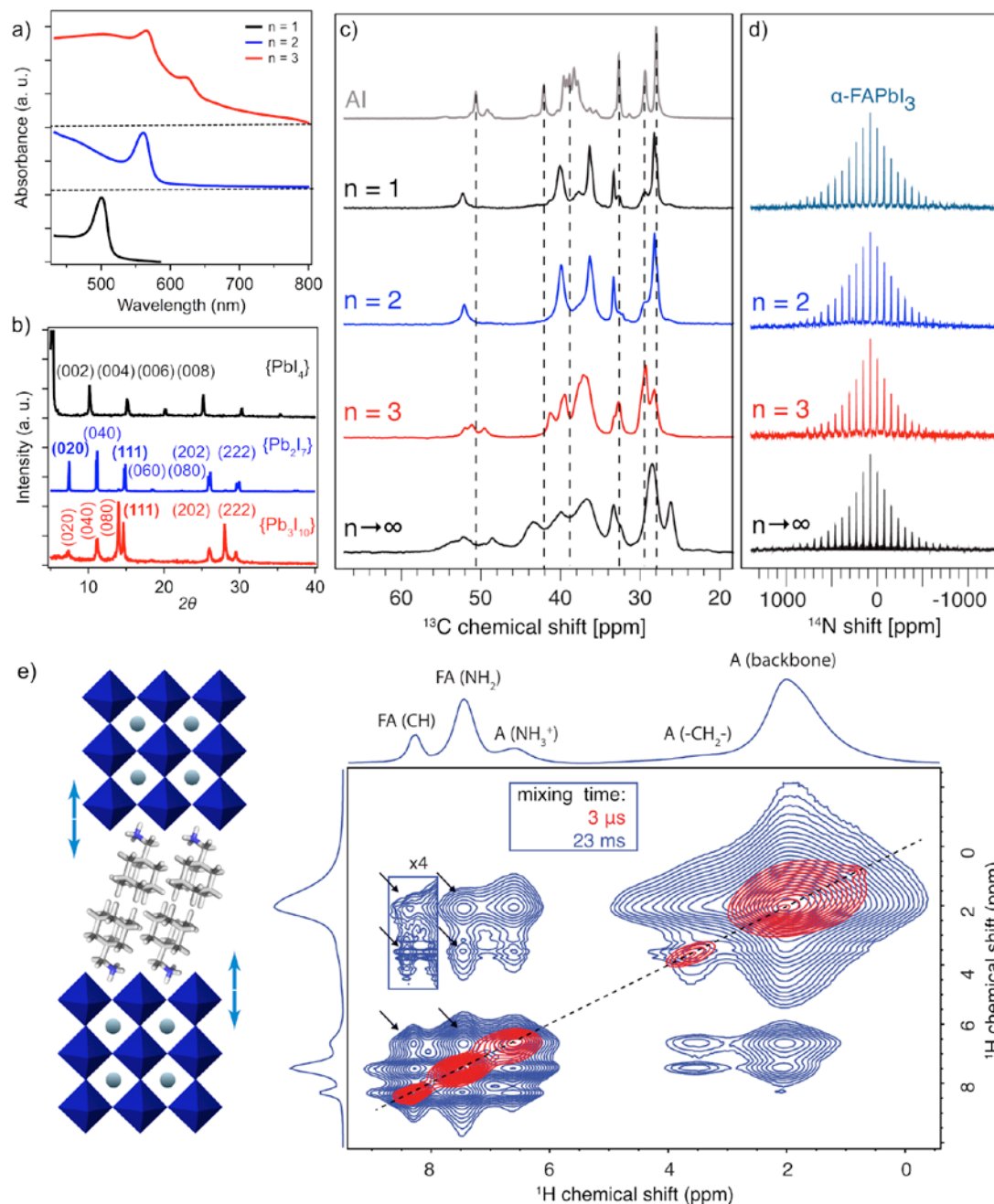
Figure 11. Hybrid layered perovskite Ruddlesden-Popper case. (a) UV-Vis absorption spectra spectra of three different $A_2FA_{n-1}Pb_nI_{3n+1}$ formulations (n = 1, 2, and 3). A = (adamantan-1-yl)methanammonium. (b) XRD patterns on glass substrates for thin films based on the $A_2FA_{n-1}Pb_nI_{3n+1}$ perovskite compositions (n = 1, 2, and 3). The indices of the corresponding planes are based on the Ruddlesden-Popper systems with comparable inorganic phases ({PbI_4} for n = 1, {Pb_2I_7} for n = 2, and {Pb_3I_{10}} for n = 3).[31] (c) ^{13}C CP solid-state MAS NMR spectra at 21.1 T, 100 K, 12 kHz MAS in the spectral area of the spacer (between 20 and 60 ppm) of neat AI and mechanochemical $A_2FA_{n-1}PbnI_{3n+1}$ (n = 1, 2, 3, →∞) powders. The n→∞ system contains a 3D α-$FAPbI_3$ perovskite powder modulated with 3 mol% AI. (d) ^{14}N solid-state MAS NMR spectra at 21.1 T, 298 K, 5 kHz of neat α-$FAPbI_3$ and $A_2FA_{n-1}Pb_nI_{3n+1}$ (n = 2, 3, →∞). CP = cross-polarization; MAS = magic angle spinning. (e) Left: Schematic of the $A_2FA_2Pb_3I_{10}$ composition. The arrows indicate the proximity between the FA cations and the backbone of the spacer, which provides a correlation observed by spin diffusion (SD) experiments. Right: ^1H-^1H SD solid state MAS NMR spectra at 21.1 T, 298 K, 20 kHz MAS of mechanochemical A2FA2Pb3I10 using mixing times of 3 μs (red) and 23 ms (blue). The formulations are defined by the stoichiometry of the precursors and they include mixtures of phases for n > 2 compositions. The region inside a rectangle is magnified to highlight the low intensity cross-peaks. The black arrows show the cross-peaks that evidence atomic-level interaction between FA and A. Adapted from ref.[87] with permission.

from n = 1 (A_2PbI_4) to n = ∞ (α-FAPbI$_3$).[31-35] In addition, as a result of high exciton binding energies, their UV-Vis absorption spectra typically show excitonic features that gradually disappear with an increase in the number of layers.[85] The UV-Vis absorption spectra of $A_2FA_{n-1}Pb_nI_{3n+1}$ (Figure 11a) show strong exciton absorption signals and a gradual red shift of the absorption with an increase in the number of layers (Figure 11a), which is suggestive of the formation of the layered structure. The excitonic absorption peaks are well defined for the n = 1–2 compositions, whereas multiple signals occur for n > 2 compositions, suggesting a mixture of different phases within a single predominant phase (Figure 11a), which is typical for layered hybrid perovskite films. There is evidence that this feature can be beneficial for the electron transfer processes of interest to optoelectronic applications.[85-86]

With analogy to the modulated perovskite systems, the atomic-level microstructure of layered 2D perovskite materials can also be assessed by solid-state NMR spectroscopy. To probe the interaction between the spacers and α-FAPbI$_3$, ^{13}C and ^{15}N MAS NMR spectra at 100 K are particularly insightful.[54-59] The analysis requires comparing the neat spacer, the 2D perovskite compositions (n = 1, 2, and 3), and the 3D phase modified with sub-stoichiometric (e.g. 3 mol%) amount of the spacer (n →∞; Figure 11c–d).[51,76] The ^{13}C NMR spectra of the (adamantan-1-yl)methanammonium spacer reveals clear differences between neat iodide salt of the spacer, layered 2D compositions, and the modified α-FAPbI$_3$ phase (Figure 11c).[87] The peaks shift and they are broadened compared to the signals of neat AI, which is in accordance with the existence of the spacer in a new chemical environment, interacting with the $[PbI_6]^{4-}$ slabs, as it would be the case in a layered structure. With the increasing of the n value, the ^{13}C resonances gradually broaden, indicating structural disorder in the FA/AI phases. This is further reflected in the ^{14}N MAS spectra (Figure 11d) of both $A_2FA_{n-1}Pb_nI_{3n+1}$ and modulated α-FAPbI$_3$ (n→∞) compositions. Unlike effective modulators shown previously, ^{14}N NMR spectra of layered 2D systems show only subtle narrowing of the SSB manifold compared to the 3D α-FAPbI$_3$ perovskite. In this case, however, for unambiguous evidence of the atomic-level contact between FA and spacer A, it is necessary to demonstrate their presence within the same microstructure at a distance on the order of 10 Å. For this purpose, two-dimensional [1]H-^{1}H spin diffusion (SD) measurements are particularly relevant (Figure 11e), as in this experiment magnetization exchange is allowed to occur during a longer mixing period, which results in a correlation between species that are within 1 nm distance.[58,87] For

instance, the SD spectrum of $A_2FA_2Pb_3I_{10}$ is symmetric around the diagonal, with the diagonal signals corresponding to those shown directly on the two projections (Figure 11e). After a mixing time of 23 ms, a series of off-diagonal peaks appear that evidence the atomic-level proximity between species. This interaction can be either intramolecular (e.g. backbone of spacer) or intermolecular (between the FA cation and the spacer). As the cross-peaks are present in the spectrum for each of the two FA environments (CH and NH_2^+), which is correlated to the chemical environments of the spacer (the backbone, -CH_2^- and -NH_3^+), this unambiguously shows that the two cations exist in the same microscopic phase.[87] The analysis of structural properties of such layered systems is complemented by X-ray diffraction (XRD), as the corresponding XRD patterns commonly reveal the presence of low-dimensional phases through the appearance of low angle reflections in the 2θ range below 10 °. Diffractograms of $A_2FA_{n-1}Pb_nI_{3n+1}$ films on microscopic glass slides show low angle reflections below 10°, typical for layered perovskite materials (Figure 11b).[31-33] While the n = 1 compositions show predominant low angle reflections around 6° associated with (002) reflections that are related to the parallel orientation with respect to the substrate, the n > 1 compositions show a lattice reflection at 2θ °15 that can be ascribed to the (111) plane, indicative of the perpendicular orientation. This orientation is of particular interest to the photovoltaic performance, as it enables effective charge extraction through the inorganic slabs.

The photovoltaic properties of the layered hybrid perovskite solar cells are therefore more effective for the higher compositional representatives (n > 1), which is also in accordance with their optical properties revealed by the UV-Vis absorption spectra (Figure 11a). Moreover, it is apparent that n ≥ 3 compositions feature an onset above 720 nm. This is indicative of the presence of additional 3D phases.[85] Despite the co-existing phases, the highest-performing devices based on $A_2FA_2Pb_3I_{10}$ composition show a short circuit current density (J_{SC}) of 14.3 mA cm^{-2}, open circuit voltage (V_{OC}) of 1.08 V, and fill factor (FF) of 0.50, resulting in a PCE of 7.8% in a reverse scan,[87] which is superior to other FA-based low-dimensional systems.[88] Furthermore, the long-term stability under full sun illumination under inert conditions at ambient temperature show that >84% of the overall PCE is maintained over more than 800 h of continuous operation at their maximum power point. Moreover, storage in humid ambient air with a relative humidity of ~50% maintains >90% of the initial PCE after 900 h. On the contrary, pristine 3D FAPbI$_3$ PSCs lose more than 50% of their performance after <200 h,[88] which empha-

sizes the potential in the performance and stabilization of layered hybrid perovskite solar cells. In this regard, the most prominent application of layered 2D perovskites is stabilization of highly efficient 3D perovskite materials.

2D/3D perovskite heterostructures are presently the most successful category of hybrid perovskite materials that meet both the performance and the stability requirements. The challenge, however, remains to retain performances comparable to the 3D PSCs with high operational stabilities in ambient air. Further engineer-

ing of organic spacer layers provides a productive platform to ascertain this potential, such as by engineering π interactions, through exploiting hydrophobic fluoroarene moieties. There are several examples of fluorine-containing aromatic spacers in layered hybrid perovskites over the past years.[77,89] For instance, a 2D FEA_2PbI_4 perovskite layer employing perfluorophenylethylammonium (FEA) as a fluoroarene cation was inserted between the 3D hybrid perovskite film and the hole-transporting material (Figure 12).[90] As a result of this overlayer, 2D/3D PSCs were shown to retain 90% of their efficiency
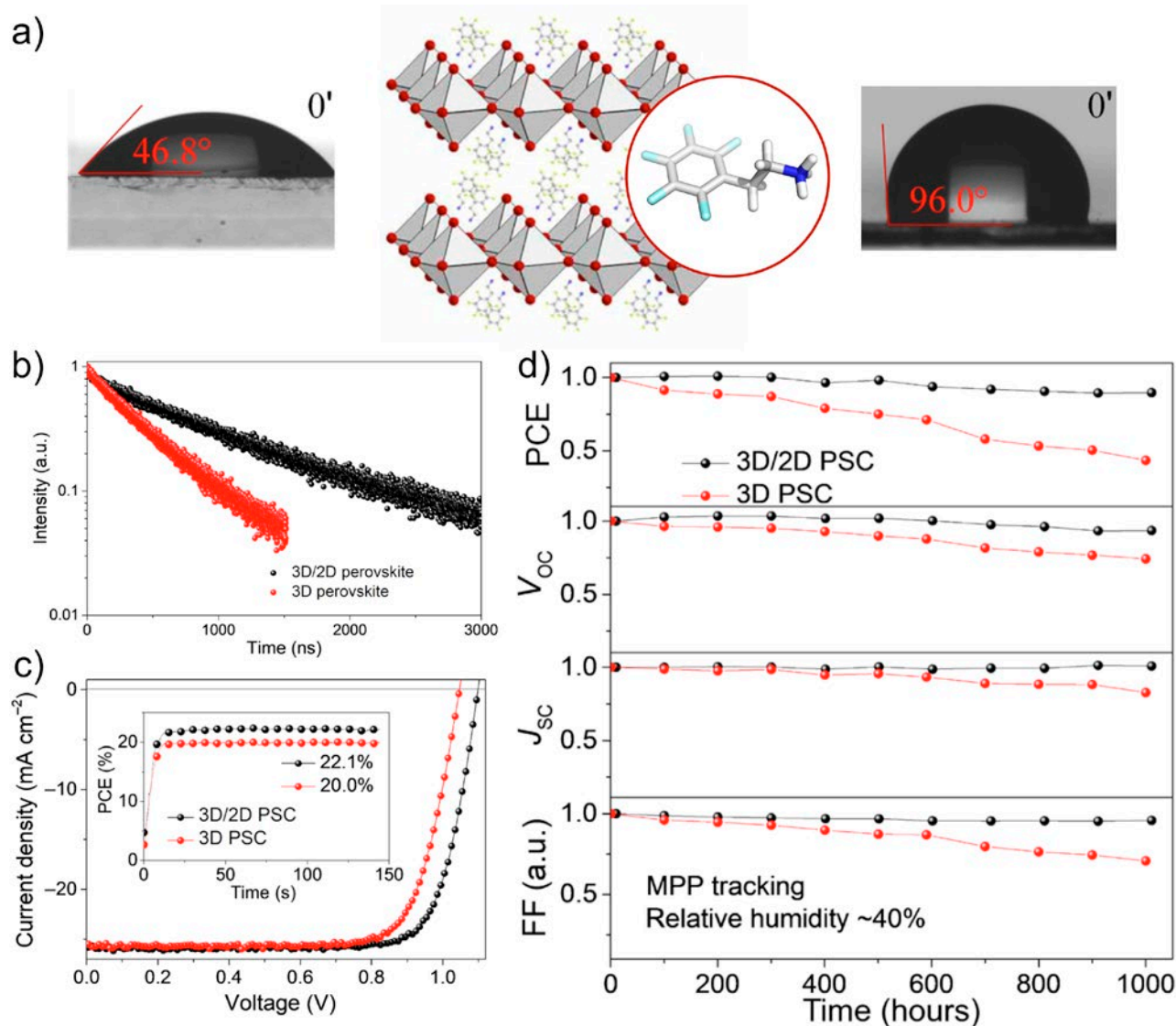
Figure 12. 2D/3D perovskite heterostructure case. (a) Schematic representation of a layered 2D perovskite structure incorporating perfluoroethylammonium (FEA) spacer layer with the contact angle measurements of the neat 3D perovskite (left) and the corresponding 2D/3D heterostructure based on the FEA overlayer (right). (b) Time-resolved photoluminescence decay traces recorded for the 3D and 2D/3D perovskite films. (c) J-V curves of a 3D PSC and a 2D/3D PSC with the maximum power point tracking shown in the inset. (d) Ambient atmosphere ageing results of the unsealed 3D and 2D/3D PSCs with the relative humidity shown in the inset. Adapted from ref.[90]

during operation for 1000 h in humid air under simulated sunlight, which is ascribed to high hydrophobicity of the system (Figure 12a,d). Moreover, the 2D layer was also shown to enhance interfacial charge-extraction, suppressing non-radiative carrier recombination (Figure 12b) and resulting in PCE >22% (Figure 12c).[90] These remarkable properties exemplify the beneficial effect of fluoroarene moieties on the structure and morphology of layered perovskite materials, as well as their heterostructures. It can be argued that such systems affect the ionic migration within the active layers of the solar cell through various ion-π interactions, which requires further investigation to exploit these molecular design concepts in the future. Such investigations, in conjunction with solid-state NMR spectroscopic analysis, could set the basis for fully exploiting the strategies of supramolecular chemistry that are effectively employed by natural systems to further advance molecular photovoltaics.

In summary, while a number of challenges with the hybrid perovskites remain to be addressed, recent developments in molecular design and atomic-level investigation open perspectives for further advancements. This is particularly the case in the context of molecular modulation and the development of layered perovskite architectures, which promise to revolutionize the field of hybrid perovskite solar cells.

4. PERSPECTIVES FOR ADVANCING DSSCS AND PSCS

Dye-sensitized and perovskite solar cells have been extensively developed over the past decade, providing sustainable solutions to present energy demands. Dye-sensitized solar cells were inspired by natural photosynthesis and they remain the most powerful technologies for harvesting ambient light to date. Their performances are complemented by an aesthetic appeal, which stimulated the first commercial applications, leading to the current yearly production in the megawatt range. This development involved a number of stages driven by molecular engineering of a variety of dyes and redox shuttles, as well as solvent-free electrolytes based on ionic liquids, fostering industrial applications. Meanwhile, their efficiency remains below the theoretical limit. It is therefore instrumental to focus on the development of solid-state dye-sensitized solar cell technologies. The basis for such systems has already been established over the past years by relying on Cu-based redox shuttles and co-sensitization with organic donor-π-acceptor dye systems. To drive this progress further, unravelling and controlling the interactions in the solid state is essential. Towards this goal, natural systems might be able to provide inspiration. This particularly refers to controlling the assembly of the dyes and redox shuttles by relying on the strategies of supramolecular chemistry, which could enable engineering side-chains of both dyes and redox-shuttles to fine-tune their contacts. This effort should be complemented by the assessment of the potential for utilizing tandem redox shuttles for directing the electron-transfer cascades. Overall, in-depth investigation of the orientation and packing in conjunction with rational supramolecular design can pave the way for overcoming the current performance limitations of dye-sensitized solar cells

On the other hand, as the performance of hybrid perovskite solar cells starts to approach theoretical limits, the research focus shifts towards resolving their stability limitations without compromising the performance. In this regard, two strategies have been particularly promising, namely the molecular modulation and the development of layered two-dimensional perovskite architectures, which was facilitated by the use of solid-state NMR spectroscopy to assess the interactions at the atomic level, setting the stage for advanced molecular design. Further advancements to overcome the challenges can be addressed by relying on the concepts of supramolecular engineering to develop novel supramolecular modulators, as well as layered perovskite materials with superior properties. As structure-property relationships are unravelled at the atomic level, a new platform for rational molecular design emerges to control the underlying processes. Here, fine-tuning the non-covalent interactions can play a major role in controlling the phase purity and orientation of layered hybrid perovskites, while facilitating the implementation of electroactive systems and controlling the ionic motion. In addition, manipulating the interactions between the perovskite and hole- and electron-transporting materials could ensure maximizing the impact of PSCs. These strategies can open the way to combining the functionality exploited in artificial supramolecular systems with solar energy conversion. We predict that this approach will play a major role in the near future, as more innovative strategies emerge to control the properties of light-harvesting materials and the corresponding solar cells.

that are providing support for the ongoing research efforts at EPFL. Furthermore, the authors are grateful to Thomas Schneeberger (University of Bern) for contributing by helpful editorial suggestions.

REFERENCE

1. S. Sorrell, *Ren. Sust. Energy Rev.* **2015**, *47*, 74–82.
2. M. Hosenuzzaman, N. A. Rahim, J. Selvaraj, M. Hasanuzzaman, A. B. M. A. Malek, A. Nahar, *Ren. Sust. Energy Rev.* **2015**, *41*, 284–297.
3. V. Balzani, A. Credi, M. Venturi, *ChemSusChem* **2008**, *1*, 26–58.
4. M. R. Wasielewski, *Chem. Rev.* **1992**, *92*, 435–461.
5. V. Balzani, M. Gómez-López, J. F. Stoddart, *Acc. Chem. Res.* **1998**, *31*, 405–414.
6. E. R. Kay, D. A. Leigh, *Angew. Chem. Int. Ed.* **2015**, *54*, 2–11.
7. S. Erbas-Cakmak, D. A. Leigh, C. T. McTernan, A. L. Nussbaumer, *Chem. Rev.* **2015**, *115*, 10081–10206.
8. B. O'Regan, M. Grätzel, *Nature* **1991**, *353*, 737–740.
9. M. Grätzel, *Nature* **2001**, *414*, 338–344.
10. M. Grätzel, *J. Photochem. Photobiol. C: Photochem. Rev.* **2003**, *4*, 145–153.
11. A. Hagfeldt, G. Boschloo, L. Sun, L. Kloo, H. Pettersson, *Chem. Rev.* **2010**, *110*, 6595–6663.
12. M. K. Nazeeruddin, E. Baranoff, M. Grätzel, *Solar Energy* **2011**, *85*, 1172–1178.
13. Y. Cao, Y. Saygili, A. Ummadisingu, J. Teuscher, J. Luo, N. Pellet, F. Giordano, S. M. Zakeeruddin, J.-E. Moser, M. Freitag, A. Hagfeldt, M. Graetzel, *Nat. Commun.* **2017**, *8*, 15390.
14. M. Grätzel, *MRS Bull.* **2005**, *30*, 23–27.
15. J.-H. Yum, P. Chen, M. Grätzel, M. K. Nazeeruddin, *ChemSusChem* **2008**, *1*, 699–707.
16. NREL Best Research Cell Efficiency Chart; available online (Accessed in August 2019).
17. W. S. Yang, B.-W. Park, E. H. Jung, N. J. Jeon, Y. C. Kim, D. U. Lee, S. S. Shin, J. Seo, E. K. Kim, J. H. Noh, S. I. Seok, *Science* **2017**, *356*, 1376–1379.
18. J.-P. Correa-Baena, M. Saliba, T. Buonassisi, M. Grätzel, A. Abate, W. Tress, A. Hagfeldt, *Science* **2017**, *358*, 739–744.
19. (a) N. Pellet, P. Gao, G. Gregori, T.-Y. Yang, M. K. Nazeeruddin, J. Maier, M. Grätzel, Angew. Chem. Int. Ed. 2014, 53, 3151–3157. (b) A. Senocrate, I. Moudrakovski, G. Y. Kim, T.-Y. Yang, G. Gregori, M. Grätzel, J. Maier, *Angew. Chem. Int. Ed.* **2017**, *56*, 7755–7759.
20. (a) M. Grätzel, *Nat. Mater.* **2014**, *13*, 838–842. (b) M. Grätzel, *Acc. Chem. Res.* **2017**, *50*, 487–491.
21. X. Li, D. Bi, C. Yi, J. D. Decoppet, J. Luo, S. M. Zakeeruddin, A. Hagfeldt, M. Grätzel, *Science* **2016**, *353*, 58–62.
22. J.-P. Correa-Baena, A. Abate, M. Saliba, W. Tress, T. J. Jacobsson, M. Grätzel, A. Hagfeldt, *Energy Environ. Sci.* **2017**, *10*, 710–727.
23. M. Saliba, J.-P. Correa-Baena, M. Grätzel, A. Hagfeldt, A. Abate, *Angew. Chem. Int. Ed.* **2018**, *57*, 2554–2569.
24. Available online.
25. M. Saliba, T. Matsui, J.-Y. Seo, K. Domanski, J.-P. Correa-Baena, M. K. Nazeeruddin, S. M. Zakeeruddin, W. Tress, A. Abate, A. Hagfeldt, M. Grätzel, *Energy Environ. Sci.* **2016**, *9*, 1989–1997.
26. M. Saliba, T. Matsui, K. Domanski, J. Y. Seo, A. Ummadisingu, S. M. Zakeeruddin, J. P. Correa-Baena, W. R. Tress, A. Abate, A. Hagfeldt, M. Grätzel, *Science* **2016**, *354*, 206–209.
27. (a) Y. H. Lee, J. Luo, R. Humphry-Baker, P. Gao, M. Grätzel, M. K. Nazeeruddin, *Adv. Funct. Mater.* **2015**, *25*, 3925–3933. (b) N. H. Tiep, Z. Ku, H. J. Fan, *Adv. Energy Mater.* **2016**, *6*, 1501420.
28. J. V. Milić, N. Arora, M. I. Dar, S. M. Zakeeruddin, M. Grätzel, *Adv. Mater. Interfaces* **2018**, *356*, 1800416.
29. T. A. Berhe, W.-N. Su, C.-H. Chen, C.-J. Pan, J.-H. Cheng, H.-M. Chen, M.-C. Tsai, L.-Y. Chen, A. A. Dubale, B.-J. Hwang, *Energy Environ. Sci.* **2016**, *9*, 323–356.
30. (a) K. Domanski, E. A. Alharbi, A. Hagfeldt, M. Grätzel, W. Tress, *Nat. Energy* **2018**, *3*, 61–67; (b) K. Domanski, J.-P. Correa-Baena, N. Mine, M. K. Nazeeruddin, A. Abate, M. Saliba, W. Tress, A. Hagfeldt, M. Grätzel, *ACS Nano* **2016**, *10*, 6306–6314.
31. H. Tsai, W. Nie, J.-C. Blancon, C. C. Stoumpos, R. Asadpour, B. Harutyunyan, A. J. Neukirch, R. Verduzco, J. J. Crochet, S. Tretiak, L. Pedesseau, J. Even, M. A. Alam, G. Gupta, J. Lou, P. M. Ajayan, M. J. Bedzyk, M. G. Kanatzidis, A. D. Mohite, *Nature* **2016**, *536*, 312–316.
32. D. H. Cao, C. C. Stoumpos, T. Yokoyama, J. L. Logsdon, T.-B. Song, O. K. Farha, M. R. Wasielewski, J. T. Hupp, M. G. Kanatzidis, *ACS Energy Let.* **2017**, *2*, 982–990.
33. J. C. Blancon, H. Tsai, W. Nie, C. C. Stoumpos, L. Pedesseau, C. Katan, M. Kepenekian, C. M. M. Soe, K. Appavoo, M. Y. Sfeir, S. Tretiak, P. M. Ajayan, M. G. Kanatzidis, J. Even, J. J. Crochet, A. D. Mohite, *Science* **2017**, *355*, 1288–1292.
34. G. Grancini, C. Roldán-Carmona, I. Zimmermann, E. Mosconi, X. Lee, D. Martineau, S. Narbey, F. Oswald, F. De Angelis, M. Grätzel, M. K. Nazeeruddin, *Nat. Commun.* **2017**, *8*, 15684.

35. Y. Chen, Y. Sun, J. Peng, J. Tang, K. Zheng, Z. Liang, *Adv. Mater.* **2017**, *131*, 1703487.

36. L. Mao, W. Ke, L. Pedesseau, Y. Wu, C. Katan, J. Even, M. R. Wasielewski, C. C. Stoumpos, M. G. Kanatzidis, *J. Am. Chem. Soc.* **2018**, *140*, 3775–3783.

37. S. Kim, J. K. Lee, S. O. Kang, J. Ko, J. H. Yum, S. Fantacci, F. De Angelis, D. Di Censo, M. K. Nazeeruddin, M. Grätzel, *J. Am. Chem. Soc.* **2006**, *128*, 16701–16707.

38. D. Casanova, F. P. Rotzinger, M. Grätzel, J. *Chem. Theory Comput.* **2010**, *6*, 1219–1227.

39. M. Katono, T. Bessho, S. Meng, R. Humphry-Baker, G. Rothenberger, S. M. Zakeeruddin, E. Kaxiras, M. Grätzel, *Langmuir* **2011**, *27*, 14248–14252.

40. (a) F. De Angelis, S. Fantacci, A. Selloni, Md.K. Nazeeruddin, M. Grätzel, *J. Phys. Chem. C* **2010**, *114*, 6054–6061; (b) F. De Angelis, S. Fantacci, A. Selloni, Md. K. Nazeeruddin, M. Grätzel, *J. Am. Chem. Soc.* **2007**, *129*, 14156–14157.

41. F. De Angelis, S. Fantacci, A. Selloni, M. Grätzel, *Nano Lett.* **2007**, *7*, 3189–3195.

42. A. Yella, H.-W. Lee, H. N. Tsao, C. Yi, A. Kumar Chandiran, Md. K. Nazeeruddin, W.-G. Diau, C.-Y. Yeh, S. M. Zakeeruddin, M. Grätzel, *Science* **2011**, *334*, 629–634.

43. S. Mathew, A. Yella, P. Gao, R. Humphry-Baker, B. F. E. Curchod, N. Ashari-Astani, I. Tavernelli, M. K. Nazeeruddin, M. Grätzel, *Nat. Chem.* **2014**, *6*, 242–247.

44. P. Bonhôte, A.-P. Dias, N. Papageorgiou, K. Kalyanasundaram, M. Grätzel, *Inorg. Chem.* **1996**, *35*, 1168–1178.

45. Y. Bai, Y. Cao, J. Zhang, M. Wang, R. Li, P. Wang, S. M. Zakeeruddin, M. Grätzel, *Nat. Mater.* **2008**, *7*, 626–630.

46. U. Bach, D. Lupo, P. Comte, J. E. Moser, F. Weissörtel, J. Salbeck, H. Spreitzer, M. Grätzel, *Nature* **1998**, *395*, 583–585.

47. M. Freitag, J. Teuscher, Y. Saygili, X. Zhang, F. Giordano, P. Liska, J. Hua, S. M. Zakeeruddin, J.-E. Moser, M. Grätzel, A. Hagfeldt, *Nat. Photonics* **2017**, *11*, 372–378.

48. Y. Rong, Y. Hu, A. Mei, H. Tan, M. I. Saidaminov, S. I. Seok, M. D. McGehee, E. H. Sargent, H. Han, *Science* **2018**, *361*, eaat8235.

49. C. H. Ng, H. N. Lim, S. Hayase, Z. Zainal, N. M. Huang, *Ren. Sust. Energy Rev.* **2018**, *90*, 248–274.

50. H. Zhang, M. K. Nazeeruddin, W. C. H. Choy, *Adv. Mater.* **2019**, *2*, 1805702.

51. J. V. Milić, D. J. Kubicki, L. Emsley, M. Grätzel, *Chimia* **2019**, *73*, 317–323.

52. G. Grancini, M. K. Nazeeruddin, *Nat. Rev. Mater.* **2019**, *4*, 4–22.

53. L. Mao, C. C. Stoumpos, M. G. Kanatzidis, *J. Am. Chem. Soc.* **2019**, *141*, 1171–1190.

54. D. J. Kubicki, D. Prochowicz, A. Hofstetter, P. Péchy, S. M. Zakeeruddin, M. Grätzel, L. Emsley, *J. Am. Chem. Soc.* **2017**, *139*, 10055–10061.

55. D. J. Kubicki, D. Prochowicz, A. Hofstetter, S. M. Zakeeruddin, M. Grätzel, L. Emsley, *J. Am. Chem. Soc.* **2017**, *139*, 14173–14180.

56. D. J. Kubicki, D. Prochowicz, A. Hofstetter, M. Saski, P. Yadav, D. Bi, N. Pellet, J. Lewiński, S. M. Zakeeruddin, M. Grätzel, L. Emsley, *J. Am. Chem. Soc.* **2018**, *140*, 3345–3351.

57. D. J. Kubicki, D. Prochowicz, A. Hofstetter, S. M. Zakeeruddin, M. Grätzel, L. Emsley, *J. Am. Chem. Soc.* **2018**, *140*, 7232–7238.

58. E. A. Alharbi, A. Y. Alyamani, D. J. Kubicki, A. R. Uhl, B. J. Walder, A. Q. Alanazi, J. Luo, A. Burgos-Caminal, A. Albadri, H. Albrithen, M. H. Alotaibi, J.-E. Moser, S. M. Zakeeruddin, F. Giordano, L. Emsley, M. Grätzel, *Nat. Commun.* **2019**, *10*, 3008.

59. M. M. Tavakoli, W. Tress, J. V. Milić, D. Kubicki, L. Emsley, M. Grätzel, *Energy Environ. Sci.* **2018**, *11*, 3310–3320.

60. A. Kojima, K. Teshima, Y. Shirai, T. Miyasaka, *J. Am. Chem. Soc.* **2009**, *131*, 6050–6051.

61. G. E. Eperon, S. D. Stranks, C. Menelaou, M. B. Johnston, L. M. Herz, H. J. Snaith, *Energy Environ. Sci.* **2014**, *7*, 982–988.

62. M. T. Weller, O. J. Weber, J. M. Frost, A. Walsh, *J. Phys. Chem. Lett.* **2015**, *6*, 3209–3212.

63. B. Conings, J. Drijkoningen, N. Gauquelin, A. Babayigit, J. D'Haen, L. D'Olieslaeger, A. Ethirajan, J. Verbeeck, J. Manca, E. Mosconi, F. De Angelis, H-G. Boyen, *Adv. Energy Mater.* **2015**, *5*, 1500477.

64. D. Prochowicz, R. Runjhun, M. M. Tavakoli, P. Yadav, M. Saski, A. Q. Alanazi, D. J. Kubicki, Z. Kaszkur, S. M. Zakeeruddin, J. Lewiński, M. Graetzel, *Chem. Mater.* **2019**, *31*, 1620–1627.

65. N. J. Jeon, J. H. Noh, W. S. Yang, Y. C. Kim, S. Ryu, J. Seo, S. Il Seok, *Nature* **2015**, *517*, 476–480.

66. N. J. Jeon, H. Na, E. H. Jung, T.-Y. Yang, Y. G. Lee, G. Kim, H.-W. Shin, S. Seok, J. Lee, J. Seo, *Nat. Energy* **2018**, *3*, 682–689.

67. Q. Jiang, Y. Zhao, X. Zhang, X. Yang, Y. Chen, Z. Chu, Q. Ye, X. Li, Z. Yin, J. You, *Nat. Photonics* **2019**, *13*, 460–466.

68. A. R. B. M. Yusoff, P. Gao, M. K. Nazeeruddin, *Coord. Chem. Rev.* **2018**, *373*, 258–294.

69. J.-P. Correa-Baena, M. Anaya, G. Lozano, W. Tress, K. Domanski, M. Saliba, T. Matsui, T. J. Jacobsson,

M. E. Calvo, A. Abate, M. Grätzel, H. Míguez, A. Hagfeldt, *Adv. Mater.* **2016**, *28*, 5031–5037.

70. A. Sharenko, M. F. Toney, *J. Am. Chem. Soc.* **2016**, *138*, 463–470.

71. J. M. Ball, A. Petrozza, *Nat. Energy* **2016**, *1*, 16149.

72. X. Zheng, B. Chen, J. Dai, Y. Fang, Y. Bai, Y. Lin, H. Wei, X. C. Zeng, J. Huang, *Nat. Energy* **2017**, *2*, 17102.

73. R. J. Stoddard, F. T. Eickemeyer, J. K. Katahara, H. W. Hillhouse, *J. Phys. Chem. Lett.* **2017**, *8*, 3289–3298.

74. W. Tress, M. Yavari, K. Domanski, P. Yadav, B. Niesen, J. P. C. Baena, A. Hagfeldt, M. Grätzel, *Energy Environ. Sci.* **2018**, *11*, 151–165.

75. K. Domanski, B. Roose, T. Matsui, M. Saliba, S.-H. Turren-Cruz, J.-P. Correa-Baena, C. R. Carmona, G. Richardson, J. M. Foster, F. De Angelis, J. M. Ball, A. Petrozza, N. Mine, M. K. Nazeeruddin, W. Tress, M. Grätzel, U. Steiner, A. Hagfeldt, A. Abate, *Energy Environ. Sci.* **2017**, *10*, 604–613.

76. D. Bi, X. Li, J. V. Milić, D. J. Kubicki, N. Pellet, J. Luo, T. LaGrange, P. Mettraux, L. Emsley, S. M. Zakeeruddin, M. Grätzel, *Nat. Commun.* **2018**, *9*, 4482.

77. B. Saparov, D. B. Mitzi, *Chem. Rev.* **2016**, *116*, 4558–4596.

78. P. Branná, M. Rouchal, Z. Prucková, L. Dastychová, R. Lenobel, T. Pospíšil, K. Maláč, R. Vícha, *Chem. Eur. J.* **2015**, *21*, 11712–11718.

79. T. Kitagawa, Y. Idomoto, H. Matsubara, D. Hobara, T. Kakiuchi, T. Okazaki, K. Komatsu, *J. Org. Chem.* **2006**, *71*, 1362–1369.

80. Y. Xue, G. A. Mansoori, *Int. J. Mol. Sci.* **2010**, *11*, 288–303.

81. M. M. Tavakoli, D. Bi, L. Pan, A. Hagfeldt, S. M. Zakeeruddin, M. Grätzel, *Adv. Energy Mater.* **2018**, *49*, 1800275.

82. T. Kitagawa, H. Matsubara, K. Komatsu, K. Hirai, T. Okazaki, T. Hase, *Langmuir* **2013**, *29*, 4275–4282.

83. W. Peng, J. Yin, K.-T. Ho, O. Ouellette, M. De Bastiani, B. Murali, O. El Tall, C. Shen, X. Miao, J. Pan, E. Alarousu, J-H. He, B. S. Ooi, O. F. Mohammed, E. Sargent, O. M. Bakr, *Nano Lett.* **2017**, *17*, 4759–4767.

84. D. Sato, T. Akutagawa, S. Takeda, S.-I. Noro, T. Nakamura, *Inorg. Chem.* **2007**, *46*, 363–365.

85. J. Liu, J. Leng, K. Wu, J. Zhang, S. Jin, *J. Am. Chem. Soc.* **2017**, *139*, 1432–1435.

86. N. Zhou, Y. Shen, L. Li, S. Tan, N. Liu, G. Zheng, Q. Chen, H. Zhou, *J. Am. Chem. Soc.* **2018**, *140*, 459–465.

87. J. V. Milić, J.-H. Im, D. J. Kubicki, A. Ummadisingu, J.-Y. Seo, Y. Li, M. A. Ruiz Preciado, M. I. Dar, S. M. Zakeeruddin, L. Emsley, M. Grätzel, *Adv. Energy Mater.* **2019**, *131*, 1900284.

88. (a) J. Yan, W. Fu, X. Zhang, J. Chen, W. Yang, W. Qiu, G. Wu, F. Liu, P. Heremans, H. Chen, *Mater. Chem. Front.* **2017**, *2*, 121–128. (b) Z. Li, M. Yang, J.-S. Park, S.-H. Wei, J. J. Berry, K. Zhu, *Chem. Mater.* **2016**, *28*, 284–292. (c) Y. Li, J. V. Milić, A. Ummadisingu, J.-Y. Seo, J.-H. Im, H.-S. Kim, Y. Liu, M. I. Dar, S. M. Zakeeruddin, P. Wang, A. Hagfeldt, M. Grätzel, *Nano Lett.* **2019**, *19*, 150–157.

89. (a) I. Garcia-Benito, C. Quarti, V. I. E. Queloz, S. Orlandi, I. Zimmermann, M. Cavazzini, A. Lesch, S. Marras, D. Beljonne, G. Pozzi, M. K. Nazeeruddin, G. Grancini, *Chem. Mater.* **2018**, *30*, 8211–8220. (b) M. E. F. Bouduban, V. I. E. Queloz, V. M. Caselli, K. T. Cho, A. R. Kirmani, S. Paek, C. Roldán-Carmona, L. J. Richter, J. E. Moser, T. J. Savenije, M. K. Nazeeruddin, G. Grancini, *J. Phys. Chem. Lett.* **2019**, *10*, 5713–5720.

90. Y. Liu, S. Akin, L. Pan, R. Uchida, N. Arora, J. V. Milić, A. Hinderhofer, F. Schreiber, A. R. Uhl, S. M. Zakeeruddin, A. Hagfeldt, M. I. Dar, M. Grätzel, *Sci. Adv.* **2019**, *5*, eaaw2543.